Methodological Remarks on CPG-Based Control of Flapping Flight

Michael Dorothy**and Soon-Jo Chung†
University of Illinois at Urbana-Champaign, Urbana, Illinois, 61801, USA

This paper is a companion to Chung[1] and explores the applications of neurobiologically inspired control systems in the form of Central Pattern Generators (CPG) to control flapping flight dynamics. We introduce two-layer CPGs to mimic current hypotheses of mammalian studies. It is shown that symmetry breaking to initiate and recover from a turning maneuver is an effective control strategy. Attempts at dissociating slow dynamics are shown and preliminary comparisons of wing motions between biological fliers and artificial CPG networks are made.

I. Introduction

Engineered flapping flight holds promise for creating biomimetic micro aerial vehicles (MAVs) flying in low Reynolds number regimes (Re$< 10^5$) where rigid fixed wings drop substantially in aerodynamic performance. MAVs are typically classified as having maximum dimensions of 15 cm and flying at a nominal speed of 1–20 m/s in tight urban environments.[2,3] Although natural flyers such as bats, birds, and insects have captured the imaginations of scientists and engineers for centuries, the maneuvering characteristics of unmanned aerial vehicles (UAVs) are nowhere near the agility and efficiency of animal flight.[4–6] Such highly maneuverable MAVs will make advances in monitoring of critical infrastructures such as power grids, bridges, and borders, as well as in intelligence, surveillance, and reconnaissance applications.

Recently, much work has been done in determining wake structure and aerodynamics of flapping animals and robots.[7–10] Averaging and linearization around hover have proven to be effective for control design of insect-scale flight, with flapping frequencies much greater than 10Hz.[11] However, for bat scale flight (*Cynopterus brachyotis* being the key example with good observational data available), the body dynamics are oscillatory on similar timescales to the flapping frequency.[12] It should be noted that this type of flight falls directly in the range for MAVs. We can then no longer apply traditional control schema for these fliers. The authors know of no literature taking a control-theoretic view of this inherently unsteady behavior and describing guaranteed closed-loop convergence criteria.

Previous work[1,13] has shown that coupled networks of Hopf oscillators on balanced graphs exhibit exponentially stable behavior in both oscillatory mode and fixed point mode. It was shown that such networks resembled central pattern generators (CPGs) that are found in the neural systems of animals. Furthermore, key mechanisms for stabilization of longitudinal motion were investigated by numerical simulation.

The key challenge is to analyze this CPG exosystem driven dynamical system. Results of this type are not found in the literature, except for simple one-dimensional systems being driven by simple one-dimensional exosystems.[14] This is because the Poincaré-Bendixson theorem can be used for such a system. The details and use of Poincaré's ideas is omitted here, but can be found in Isidori and Byrnes[14] or Strogatz.[15] Numerical continuation methods[16] can search out parameter space, but face two difficulties. Continuation of periodic orbits requires prior knowledge of such a periodic solution for one set of parameters. We thus need a stable numerical solution a priori that is close in parameter space to the region we would like to learn about. Additionally, stability calculations in continuation rely on linearized maps at Poincaré sections. Questions

*Research Assistant, Aerospace Engineering, dorothy1@illinois.edu.
†Assistant Professor of Aerospace Engineering, Senior Member AIAA, Phone: 217-244-2737, sjchung@illinois.edu.

concerning regions of attraction are left unanswered; such questions are vital to swift maneuvers or gait changes.

The challenge is enhanced when we begin to include feedback into the CPG system. Figure 1 shows a schematic for how sensory feedback can be fed back to the CPG network. This was done in previous work for stability purposes,[1] and is also used in this paper. However, closing the loop takes what is, at best, a four-dimensional flight dynamics system with a three-dimensional driving exosystem and turns it into, at best, a still complicated four-dimensional oscillatory system. The actual models used are more complicated, but see Appendix A for the simplest form. In the absence of analytical tests and descriptions of the omega limit sets for sets of initial conditions, numerical studies are performed to identify characteristic behavior and potential challenges.

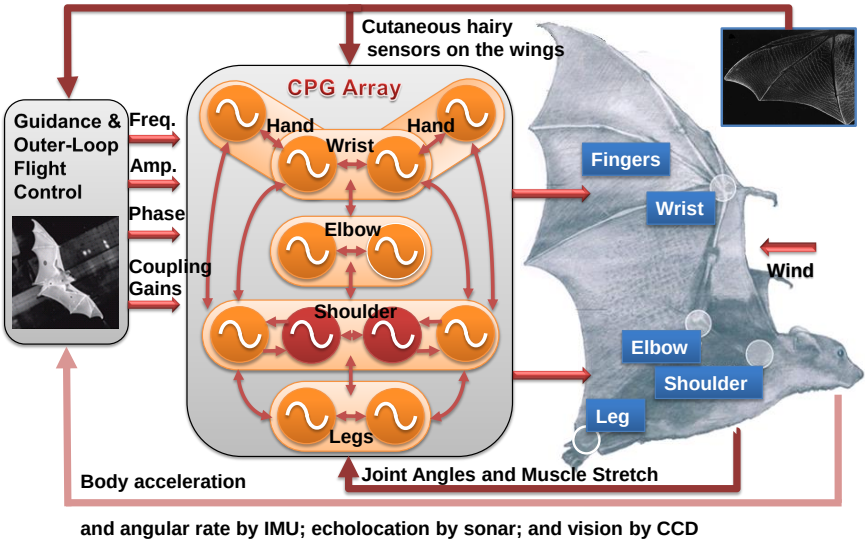

Figure 1. Control structures with the main controller and the CPG network. The outer-loop flight control modulates the rhythmic patterns (frequency, amplitude, phase lag, coupling gains) of the CPG network, without the need for directly controlling a multitude of joints.

We review the relevant key ideas in Section II. In Section III, we extend those results to include a full six degree of freedom simulation. In Section IV, we describe preliminary results from extracting slow dynamics from the highly oscillatory true dynamics. In Section V, we also compare the wing motions, in particular the wingtip motions, to published wingtip motions of live bats[12] and lay the groundwork for closer mimicry by describing a second joint. Concluding remarks are presented in Section VI.

II. Hopf Oscillators, CPGs, and Dynamical Equations

II.A. Hopf Oscillator Networks

Our neurobiologically inspired approach centers on deriving an effective mathematical model of CPGs based on coupled nonlinear limit cycle dynamics. Once neurons form reciprocally inhibiting relations, they oscillate and spike periodically. An abstract mathematical model of complicated neuron models can be obtained by coupled nonlinear limit cycles that essentially exhibit the rhythmic behaviors of coupled neuronal networks. In the field of nonlinear dynamics, a limit cycle is defined as an isolated closed trajectory that exhibits self-sustained oscillation.[15,17] If *stable*, small perturbations (initial conditions) will be forgotten and the trajectories will converge to the limit cycle. This superior robustness makes a limit cycle an ideal simplified dynamic model of CPGs.

Following Chung,[1] we use the following limit-cycle model called the Hopf oscillator, named after the

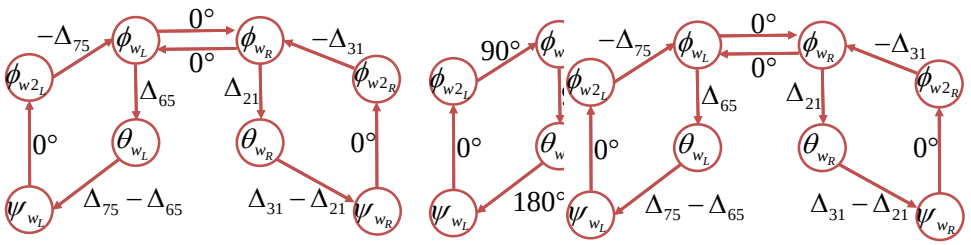

(a) Configuration A (b) Symmetric Configuration A (c) Configuration B

Figure 2. Graph configurations of the coupled Hopf oscillators on balanced graphs. Many other configurations are permitted in this paper and the unidirectional couplings can be replaced by the bi-directional couplings. The numbers next to the arrows indicate the phase shift Δ_{ij} from the i-th member to the j-th member while Figure b shows the nominal values of the phase shift from the symmetric wing configuration such that $\Delta_{21} = \Delta_{65}$=90 deg. and $\Delta_{31} = \Delta_{75} = -90$ deg. Such phase shifts define flight modes (wing movement gaits).

supercritical Hopf bifurcation model with $\sigma = 1$:

$$\frac{d}{dt}\begin{pmatrix} u-a \\ v \end{pmatrix} = \begin{bmatrix} -\lambda\left(\frac{(u-a)^2+v^2}{\rho^2} - \sigma\right) & -\omega(t) \\ \omega(t) & -\lambda\left(\frac{(u-a)^2+v^2}{\rho^2} - \sigma\right) \end{bmatrix}\begin{pmatrix} u-a \\ v \end{pmatrix} + \mathbf{u}(t) \tag{1}$$

$$\text{Equivalently,} \quad \dot{\mathbf{x}} = \mathbf{f}(\mathbf{x};\rho;\sigma) + \mathbf{u}(t), \quad \text{with} \quad \mathbf{x} = (u-a, v)^T$$

where the $\lambda > 0$ denotes the convergence rate to the symmetric limit circle of the radius $\rho > 0$ and $\mathbf{u}(t)$ is an external or coupling input. For a single Hopf oscillator with $\mathbf{u}(t) = 0$, a Lyapunov function $V = \left(\frac{(u-a)^2+v^2}{\rho^2} - 1\right)^2$ can be used to prove global asymptotic stability to the circular limit cycle. When the bifurcation parameter σ becomes negative, the stable limit cycle dynamics changes to the dynamics with a globally stable equilibrium point at the bias "a" (see [15]). Such a change can be used to turn the flapping oscillatory motion to the gliding mode, for example by changing $\sigma = 1$ to $\sigma = -1$.

The possibly time-varying parameter $\omega(t) > 0$ determines the oscillation frequency of the limit cycle. A time-varying $a(t)$ sets the bias to the limit cycle such that it converges to $u(t) = \rho\cos(\omega t + \delta) + a$ and $v(t) = \rho\sin(\omega t + \delta)$ on a circle. This bias "a" does not change the results of the stability proof. The output variable to generate the desired oscillatory motion of each joint is the first state u from the Hopf oscillator model in Eq. (1).

Synchronization means an exact match of the scaled amplitude or the frequency in this paper. Hence, phase synchronization permits different actuators to oscillate at the same frequency but with a prescribed phase lag. In essence, each CPG dynamic model in Eq. (1) is responsible for generating the limiting oscillatory behavior of a corresponding joint, and the diffusive coupling among CPGs reinforces phase synchronization. For example, the flapping angle has roughly a 90-degree phase difference with the pitching joint to maintain the positive angle of attack (see the actual data from birds in [4]). The oscillators are connected through diffusive couplings, and the i-th Hopf oscillator can be rewritten with a diffusive coupling with the phase-rotated neighbor.

$$\dot{\mathbf{x}}_i = \mathbf{f}(\mathbf{x}_i;\rho_i) - k\sum_{j\in\mathcal{N}_i}^{m_i}\left(\mathbf{x}_i - \frac{\rho_i}{\rho_j}\mathbf{R}(\Delta_{ij})\mathbf{x}_j\right) \tag{2}$$

where the Hopf oscillator dynamics $\mathbf{f}(\mathbf{x}_i;\rho_i)$ with $\sigma = 1$ is defined in Eq. (1), $\mathcal{N}_i$ denotes the set that contains only the local neighbors of the i-th Hopf oscillator, and m_i is the number of the neighbors. The 2×2 matrix $\mathbf{R}(\Delta_{ij})$ is a 2-D rotational transformation of the phase difference Δ_{ij} between the i-th and j-th oscillators. The positive (or negative) Δ_{ij} indicates how much phase the i-th member leads (or lags) from the j-th member and $\Delta_{ij} = -\Delta_{ji}$. The positive scalar k denotes the coupling gain.

Such phase shifts along with the bifurcation parameter σ can be used to define different **flight modes**, similar to **walking gaits**. Numerous configurations are possible as long as they are on balanced graphs[18] and we can choose either a bidirectional or a uni-directional coupling between the oscillators. The numbers next to the arrows indicate the phase shift Δ_{ij}, hence $\Delta_{ij} > 0$ indicates how much phase the i-th member leads. Since the graphs in Figure 2 are on balanced graphs, the number of input ports equal the number of

output ports. Further, all the phase shifts (Δ_{ij}) along one cycle should add up to a modulo of 2π. Figure 2b shows the nominal values of the phase shift from the symmetric wing configuration such that $\Delta_{21} = \Delta_{65} = 90$ deg. and $\Delta_{31} = \Delta_{75} = -90$ deg. The empirical data suggest that the pitching angle (θ_w) has approximately a 90-degree phase lag with the flapping angle (ϕ_w), which agrees with the aerodynamically optimal value.[4,7] For hovering flight, Dickison,[7] using his Robofly testbed and numerical simulations, found that increasing the phase difference value Δ_{21} to 90 deg $+\delta$ further contributed to enhancing the lift generation, which is explained by the wake capture and rotational circulation lift mechanism. Hence, the ability to control Δ_{21} allows us to investigate the optimal value of the phase difference. In addition, the nominal value of $\Delta_{31} = -90$ deg, the phase difference between the flapping stroke angle and lead-lag angle will results an elliptical orbit of the wing. On the other hand, by having two difference phase differences for the left and right wings, we can investigate how symmetric-breaking wing rotations contribute the agile turning of flapping flight.

II.B. CPGs, Conformal Mapping, and Comparison to Split-Cycle

Much work has been done to identify actual CPG-type behavior in animals. This includes results involving fish,[19] eels,[20] and cats.[21] Relatively less work has been done for mammals as compared to nonmammals. However, mammal CPG work is increasing rapidly. In this recent work, the proposal has been put forth that there should be a two-layer model rather than a one-layer model for mammalian CPGs (swimming animals exhibit behavior more resembling one-layer CPGs).[22,23] That is, instead of viewing the controller as a single central pattern generator, we view a distinction between a rhythm generator and a pattern generator. Evidence points toward the rhythm generation layer as being an emergent network of coupled oscillators, similar to what is proposed in this work. These rhythm generators may be identical, which would again fit well with our model. Then, pattern generation would be handled by a second layer. Suppose each joint's actuation has a unique waveform that is repeated in concert with the general motion. The pattern generation layer would take the simple rhythmic signal from the rhythm generator and output the correct motion waveform. Figure 3 shows a schematic of an open-loop two-layer CPG. The rhythm generators are modeled as coupled Hopf oscillators. Then the signals go to unique pattern generators which produce the uniquely desired waveform. We propose that such a pattern generation layer can be easily formed using conformal mapping.

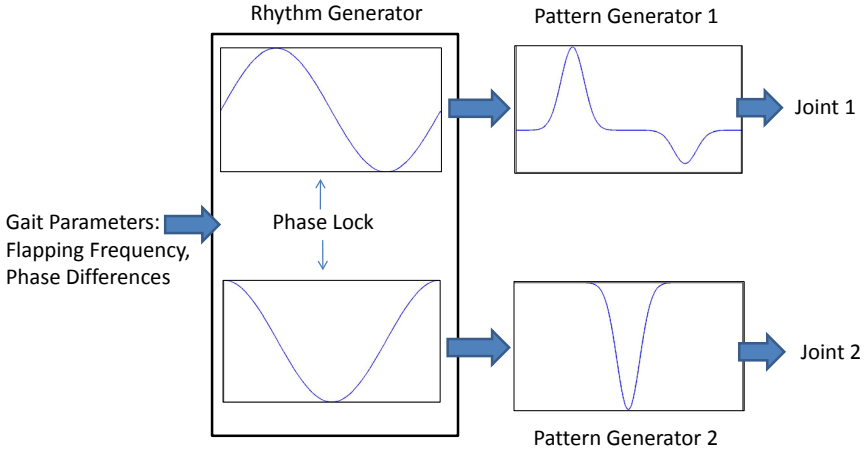

Figure 3. Schematic of open-loop CPG highlighting a distinction between rhythm generation and pattern generation.

The limit set of a particular Hopf oscillator is a simple closed curve in the plane. It is topologically similar to any other simple closed curve in the plane. Therefore, one can define a diffeomorphism as a pattern generator which can take the output of a Hopf oscillator and map it to the appropriate waveform for the particular motion being actuated. This type of mechanism gives a lot of freedom to a control designer for a robotic system. For example, consider one such waveform being used in control literature for flapping flight: split-cycles. The idea is to speed up the downstroke and delay the upstroke while keeping the overall frequency fixed. This type of design can be handled two ways by our method. One could use a single-layer CPG network and simply send a square wave as frequency input. Alternatively, one could use a double-layer CPG network and design a pattern generator to reproduce such waveforms. Furthermore, as

optimization work is done on particular waveforms, the more complicated results could be very quickly and easily implemented into a pattern generation layer model. Figure 4 shows the first method of producing a split-cycle waveform with the more general Hopf oscillator. Doman[11] showed that intra-wingbeat frequencies $\delta > 0$ and $\sigma = \frac{\delta\omega}{\omega - 2\delta}$ can be used to impede/advance each stroke without affecting the overall frequency. The sign of v in the Hopf oscillator provides information for whether it is in the upstroke or downstroke. Therefore, we use

$$\Omega = \begin{cases} \omega - \delta & \text{if } v > 0, \\ \omega + \sigma & \text{if } v < 0 \end{cases} \tag{3}$$

for the input frequency and are able to reproduce the split-cycle. Each waveform was produced by an independent trial and the difference in periods was on the order of 10^{-15}, which is considered numerical error. Thus, the Hopf oscillator model can be considered a generalization of the split-cycle.

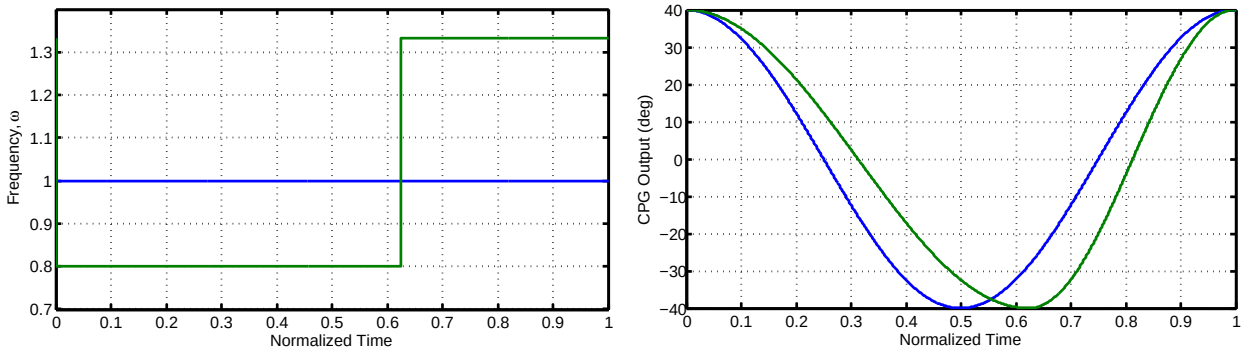

(a) Input frequency.

(b) Waveform comparison.

Figure 4. Production of split-cycle waveform via Hopf generalization.

II.C. Dynamical Equations

For simulation purposes, following Chung,[1] we calculate the local flow velocity by

$$\begin{pmatrix} V_{wx} \\ V_{wy} \\ V_{wz} \end{pmatrix} = \mathbf{T}_{ws}(\phi_w, \psi_w)\mathbf{T}_{sb}(\Theta_s)\mathbf{V}_b + \left(\mathbf{T}_{ws}(\phi_w, \psi_w) \begin{pmatrix} -\cos\psi_w \dot{\phi}_w \\ \sin\psi_w \dot{\phi}_w + \dot{\Theta}_s \\ -\dot{\psi}_w \end{pmatrix} \right) \times \begin{pmatrix} 0 \\ r \\ 0 \end{pmatrix}. \tag{4}$$

Then, we can obtain the local incident angle β_w (measured clockwise), the angle of attack α_w, and the speed of the wind V_r on the blade element on the right wing as follows

$$\begin{aligned} \beta_w(r,t) &= \tan^{-1}\frac{-V_{wz}}{V_{wx}}, \quad \alpha_w(r,t) = \theta_w(t) - \beta_w(r,t) \\ V_r^2(r,t) &= \sqrt{V_{wx}^2 + V_{wz}^2}. \end{aligned} \tag{5}$$

The seminal paper by Dickinson[7] used a hovering pair of wings without a forward speed as follows

$$\begin{aligned} C_L(\alpha_w) &= 0.225 + 1.58\sin(2.13\alpha_w - 7.2\,\text{deg}) \\ C_D(\alpha_w) &= 1.92 - 1.55\cos(2.04\alpha_w - 9.82\,\text{deg}) \end{aligned}. \tag{6}$$

From the quasi-steady approximation, we can compute the lift and drag forces acting on the blade element with width dr as follows.

$$dL = \frac{1}{2}\rho C_L\left(\alpha_w(r,t)\right)c(r)V_r^2(r,t)dr, \quad dD = \frac{1}{2}\rho C_D\left(\alpha_w(r,t)\right)c(r)V_r^2(r,t)dr \tag{7}$$

In addition, Ellington[24] derived the wing circulation $\Gamma_r = \pi\dot{\alpha}c^2(3/4 - \hat{x}_0)$ based on the Kutta-Joukowski condition. This quasi-steady approximation for the rotational lift can be written as

$$dL_{rot} = \frac{1}{2}\rho\left(2\pi(\frac{3}{4} - \hat{x}_0)\right)c^2(r)V_r(r,t)\dot{\alpha}_w dr \tag{8}$$

where $\hat{x}_0$ is the location of the pitch axis along the mean chord length. Also, $\dot{\alpha}_w$ can be computed from Eq. (5) and often approximated reasonably well by the angular rate of the wing pitch motion $\dot{\theta}_w$.

The total x and z directional forces of a single wing (either right or left) in the body frame are obtained as

$$F_{wz} = \int_{r=0}^{R} dD \sin\beta_w - (dL + dL_{rot})\cos\beta_w, \quad F_{wx} = \int_{r=0}^{R} -(dL + dL_{rot})\sin\beta_w - dD\cos\beta_w \tag{9}$$

where the positive direction of z_b is downward.

The F_{wx} and F_{wz} forces on the wing frame given in Eq. (9) can be transformed into the forces in the vehicle body frame:

$$\mathbf{F}_{\text{right}} = \begin{pmatrix} F_x \\ F_y \\ F_z \end{pmatrix}_{\text{right}} = \mathbf{T}_{bs}(\Theta_s)\mathbf{T}_{sw}(\phi_w, \psi_w) \begin{pmatrix} F_{wx} \\ 0 \\ F_{wz} \end{pmatrix}_{\text{right}} \tag{10}$$

where we added the subscript *right* to indicate the right wing. A similar expression can be obtained for the left wing ($\mathbf{F}_{\text{left}}$). Each wing has different wing angular parameters such as ϕ_w, ψ_w, and θ_w, although the stroke plane angle Θ_s is the same for both wings.

In order to compute the rotational moments generated by the aerodynamic forces, we first calculate the position of the wing blade element with respect to the body frame

$$\mathbf{p}(r) = \mathbf{T}_{bs}(\Theta_s)\mathbf{T}_{sw}(\phi_w, \psi_w) \begin{pmatrix} 0 \\ r \\ 0 \end{pmatrix} + \begin{pmatrix} d_x \\ d_y \\ d_z \end{pmatrix} \tag{11}$$

Then, we can compute the aerodynamic moments with respect to the c.g.

$$\begin{pmatrix} dM_x \\ dM_y \\ dM_z \end{pmatrix} = \mathbf{p}(r) \times \left(\mathbf{T}_{bs}(\Theta_s)\mathbf{T}_{sw}(\phi_w, \psi_w) \begin{pmatrix} -(dL + dL_{rot})\sin\beta_w - dD\cos\beta_w \\ 0 \\ dD\sin\beta_w - (dL + dL_{rot})\cos\beta_w \end{pmatrix} \right) + \begin{pmatrix} dM_{x0} \\ dM_{y0} \\ dM_{z0} \end{pmatrix} \tag{12}$$

$$\begin{pmatrix} dM_{x0} \\ dM_{y0} \\ dM_{z0} \end{pmatrix} = \mathbf{T}_{bs}(\Theta_s)\mathbf{T}_{sw}(\phi_w, \psi_w)\mathbf{T}_{\theta_w}(\theta_w)\frac{1}{2}\rho V_r^2 c(r)dr \begin{pmatrix} rc_{l0} \\ c(r)(c_{m0} + c_{m\alpha,w}\alpha_w) \\ rc_{n0} \end{pmatrix} \tag{13}$$

$$M_x = \int_{r=0}^{R} dM_x, \quad M_y = \int_{r=0}^{R} dM_y, \quad M_z = \int_{r=0}^{R} dM_z \tag{14}$$

where dM_{x0}, dM_{x0}, and dM_{x0} denote the constant aerodynamic moments that include the moment at the mean aerodynamic center, computed by the moment coefficients c_{l0}, c_{m0}, $c_{\alpha,w}$, and c_{n0}. The transformation matrix $\mathbf{T}_{\theta_w}(\theta_w)$ rotates the wing frame about the y_w axis by the wing pitch rotation angle θ_w.

We assume the mass and the moment of inertia of the wing compared to the body weight are negligible so that the c.g. remains fixed. Then, the translational motion of the c.g. of the flapping flying vehicle driven by the aerodynamic force terms in Eq. (10) can be expressed as

$$m\dot{\mathbf{V}}_b + m\mathbf{\Omega}_b \times \mathbf{V}_b = \mathbf{T}_{be}(\phi_b, \theta_b, \psi_b)\mathbf{F}_g + \mathbf{F}_{\text{right}} + \mathbf{F}_{\text{left}} + \mathbf{A} \tag{15}$$

where all the symbols are defined in the nomenclature section, and the Euler angular transformation matrix $\mathbf{T}_{be}(\phi_b, \theta_b, \psi_b)$ determines the orientation of the body frame with respect to the inertial frame. Each wing has different wing angular parameters such as ϕ_w, ψ_w, and θ_w, although the stroke plane angle Θ_s is the same for each wing.

The equations of rotational motion are driven by the aerodynamic moments $\mathbf{M}_{\text{right}}$ and $\mathbf{M}_{\text{left}}$ of each wing that can be obtained from Eq. (12)

$$\mathbf{I}_b\mathbf{\Omega}_b + \mathbf{\Omega}_b \times (\mathbf{I}_b\mathbf{\Omega}_b) = \mathbf{M}_{\text{right}} + \mathbf{M}_{\text{left}} + \mathbf{B} \tag{16}$$

The relationship between the body angular rate $\mathbf{\Omega}_b = (p, q, r)^T$ and the Euler angle vector $\mathbf{q}_b = (\phi_b, \theta_b, \psi_b)^T$ can be determined by[1]

$$\dot{\mathbf{q}}_b = \mathbf{Z}(\mathbf{q}_b)\mathbf{\Omega}_b \tag{17}$$

where any other orientation representations such as quaternions can be used in lieu of the Euler angles in the preceding equations. Also, any disturbance force and torque can be added to the equations.

Chung[1] showed that the longitudinal dynamics can be controlled without using aerodynamic control surfaces such as ailerons, elevators, rudders, and directional control of tail wings. For gliding flight, nonzero gains were used for PID control of flapping angle and lead-lag bias. Only integral control was used for pitch bias, in order to obtain a constant wing angle of attack. For flapping flight, flapping frequency and the phase difference between the lead-lag CPG and the pitching CPG were used to stabilize flight. Next, we extend this simulation to include lateral motion.

III. Six Degrees of Freedom Simulation

If we select graph configuration A in Fig. 2, we have four available phase differences. We use two degrees of freedom as follows. We do not break symmetry in lead-lag phase differences, setting

$$\Delta_{75} - \Delta_{65} = \Delta_{31} - \Delta_{21}. \tag{18}$$

We now control $\Delta_{31} - \Delta_{21}$ with proportional control and body pitch as the input. That is, we set

$$\Delta_{76} = \Delta_{75} - \Delta_{65} = \Delta_{32} = \Delta_{31} - \Delta_{21} = -K_{\Delta_{32}}\theta_b + \Delta_0. \tag{19}$$

Not only is this effective in stabilizing the longitudinal motion, the nominal value can be used to select ascent or decent angle. In order to control pitch symmetry breaking with one parameter, consider Δ as the constant nominal value (90°) of Δ_{21} and Δ_{65}. Then, set

$$\Delta_{65} = \Delta + \delta, \quad \Delta_{21} = \Delta - \delta. \tag{20}$$

The phase difference between flapping and pitch is vital for lift and thrust generation. Therefore, this difference between the right and left wings causes roll and proverse yaw. This method of symmetry breaking was observed by Hedrick and Biewener.[25]

The second method of symmetry breaking we use is lead-lag amplitude. We set this proportional to yaw rate to provide yaw rate damping. Due to the coupled nature of the motions, this causes yaw rate and roll angle to go to zero. The simulation results below follow these control laws, as well as those in the previous paper[1] for longitudinal stability.

Table 1. Simulation parameters

m=0.3kg	$\mathbf{I}_b$= 0.0012*eye(3) kgm^2	R=0.32 m	c= 0.15 m	$c_{m0} = -0.5$
k=50 or 0	λ= 10 or 50	$\rho_1 = \phi_{w,max}$=50°	$\rho_2 = \theta_{w,max}$=30°	$\rho_3 = \psi_{w,max}$=15°
$a_1 = a_5$=0	$a_2 = a_6$=0°	$a_3 = a_7$=-5°	Θ_s=20°	

The vehicle begins in a gliding mode, transitions to slowly ascending flapping flight, then executes a turn. Transition states are not well explored. As seen in the next paragraph, most transitions involve discontinuities which could be avoided in a more sophisticated control law. Most troublesome is the transition from gliding to flapping, as the body angle of attack nears −90°. Remarkably, the flapping mode corrects this transitory mode and should be a testament to the potential of our overall scheme.

To turn, at the 10 second mark, we set $\delta = 3°$, accompanied by setting $\dot{\omega} = 0$, shifting the zero point and scaling the proportional feedback for lead-lag coupling, scaling the derivative feedback for lead-lag coupling, and turning off yaw damping due to lead-lag amplitude symmetry breaking. At the 15 second mark, we return $\delta = 0°$. What is interesting here is that we have symmetric flapping, and the vehicle settles into a nice banked turn. The bank angle, rate of turn, and qualitative characteristic (e.g. amplitude of body pitch oscillation) of the turn are interestingly linked to the scale and shift of the lead-lag coupling, but an exact correlation is not yet known. This must be further investigated and understood in order to implement a better nonlinear control law. Finally, at the 20 second mark, we return the original scaling to proportional feedback of lead-lag coupling, but select a new zero point for proportional feedback and also a new scaling for derivative feedback. At this point, we also turn on yaw damping by lead-lag amplitude symmetry breaking. The roll angle through the turn is about 40° and the average global yaw rate is between 90 and 100°/*sec*. This is feasible in light of experimentation.[25]

Figure 6b shows the resulting oscillatory behavior of the flapping (ϕ_w), pitch (θ_w), and lead-lag motion (ψ_w) commanded by the CPG network and highlights the effects of our changing control variables on CPG behavior. From arbitrary initial conditions, the CPG network synchronizes globally and exponentially, indicated by the synchronization errors defined as the first element of $(\mathbf{x}_i - R(\Delta_{ij})\rho_i/\rho_j\mathbf{x}_j)$– see Fig. 6b. When the phase difference Δ_{ij} is time-varying, there is a small residual error in the synchronization ($\leq \pm 0.2^\circ$), but still effectively small. Otherwise, the synchronization errors tend exponentially to zero as predicted by Chung.[1]

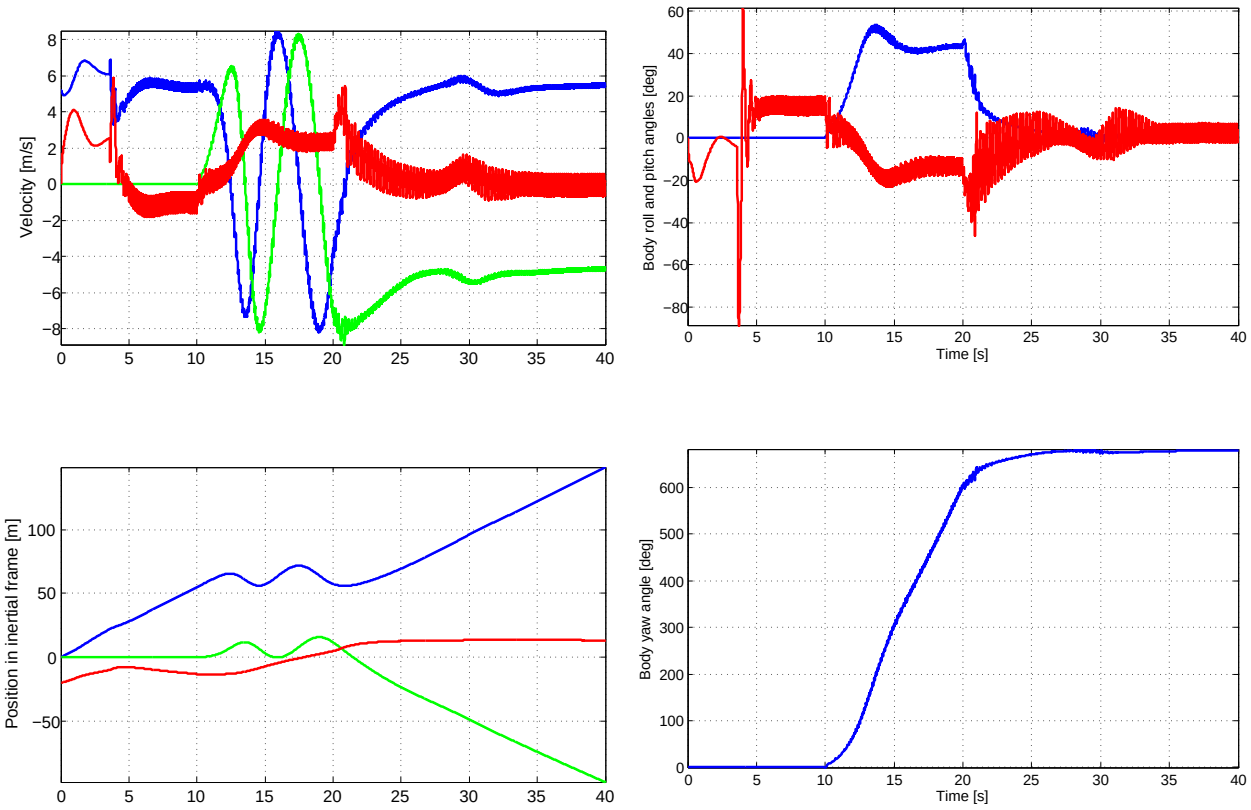

(a) Velocity and position in the inertial frame.

(b) Euler Angles

Figure 5. State vectors of the two alternating flight modes, flapping and gliding.

IV. Slow Dynamics as Reduced System

A full understanding of the convergent behavior of this oscillatory system is still unsolved. With precisely known periodic orbits, numerical continuation methods can provide changes in periodic behavior in parameter space and Lyapunov exponents can give us local convergence behavior. However, the larger picture of the slow dynamics is quite important. The authors are not aware of a global method that captures the relevant behavior. In order to investigate this problem, we present preliminary results of trying to extract the slow dynamics from a highly oscillatory simulation.

The goal is to be able to treat CPG parameters like inputs for a typical input-output system. We consider three types of preliminary tests and move from the most promising to the least promising. First, we want input parameters for the CPG network to be designable from simple ideas and for such choices to have the desired result on the resultant system. Figure 7 shows an example from this type of study. We set a desired forward velocity and then perform root-finding to determine which value of bias for flapping/lead-lag phase difference gives steady-level flight. The goal is that the system behaves in a way the makes sense: as the desired forward velocity is higher, the appropriate action is to flap faster (increase in omega) and reduce the bias for flapping/lead-lag phase difference. Figure 7 shows that it does. Many such simulations have shown similar results with different parameters, but neither one nor one hundred could confirm the hope, only disprove it and force us to reconsider.

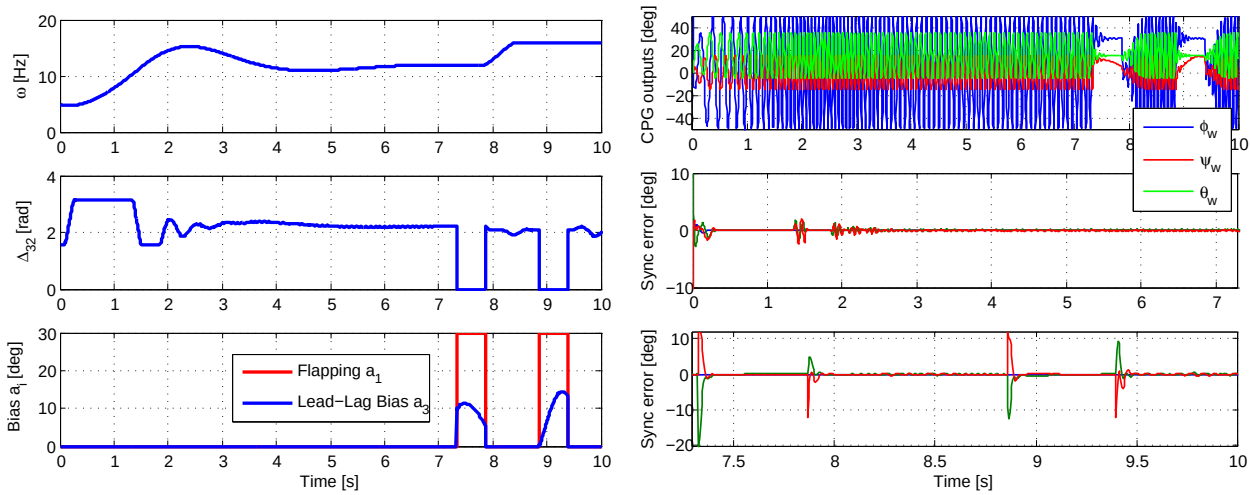

(a) Control inputs

(b) CPG array output and synchronization errors

Figure 6. State vectors of the two alternating flight modes, flapping and gliding.

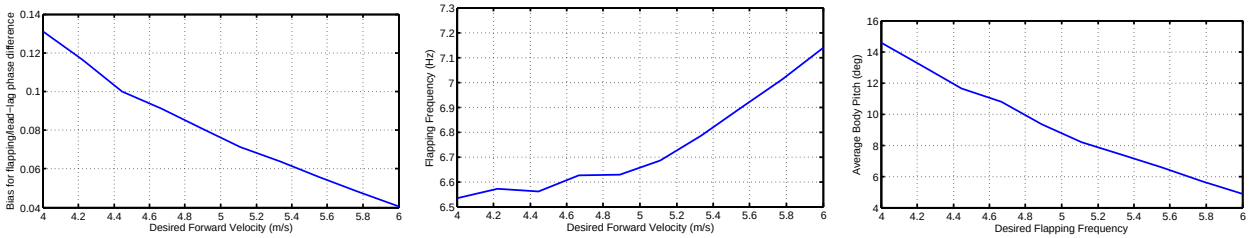

(a) Trim bias constant.

(b) Trim flapping frequency.

(c) Trim vehicle pitch.

Figure 7. Steady-state behavior.

Secondly, recall that the goal is to treat the slow dynamics as an input-output system with simple inputs being those top-level inputs to the CPG network. The test is then that the value and character of the output can depend only on fixed values of inputs. Again we focus on the longitudinal modes with the inputs being flapping frequency and the bias for flapping/lead-lag phase difference. We took two types of changes in input: steps and ramps. A random generator was used to determine the length of ramps. Fast Fourier transforms and steady-state averages were computed before and after the changes in parameters. It was found that the steady-state character, both in average value and in frequency breakdown, nearly always depended only on the steady-state input values. There appeared to be discrete values which would excite slower harmonics. No small region around these values could be found with exhibited similar behavior. This might be considered a numerical anomaly, or it might be the sign of something dangerous occurring.

The key to this final investigation is extracting simple signals from a very oscillatory one. In order to do so, we take each fast period and extract a maximum, minimum, and average. Each of these single signals then looks like a canonical second-order system. Figure 8 is an example. Therefore, we make the assumption that they can each be modeled as such and perform a nonlinear least squares fit for a general second-order system excited by an impulse. This method gives rise to all the convergence problems associated with nonlinear least squares fitting. This is very noticeable in a few solution points which differ substantially from the general trend due to fitting problems.

Figure 9 shows the results of nonlinear least squares fit for body forward velocity, vertical velocity, and pitch angle. Each subfigure contains three sets of plotted values, representing the signals due to the extraction of the maximum, minimum, and average. Only the most relevant plots, the eigenvalues of the fitted system and the steady-state value, are shown. The flapping/lead-lag bias constant is varied in each test, in order to test the idea that such inputs may be considered as inputs for designing a simple input-output model for slow dynamics. It is apparent that such parameters can have exactly the intended affect on slow behavior. There is an obvious nonlinearity occurring near the low region. There is an obvious set of trends for the eigenvalues,

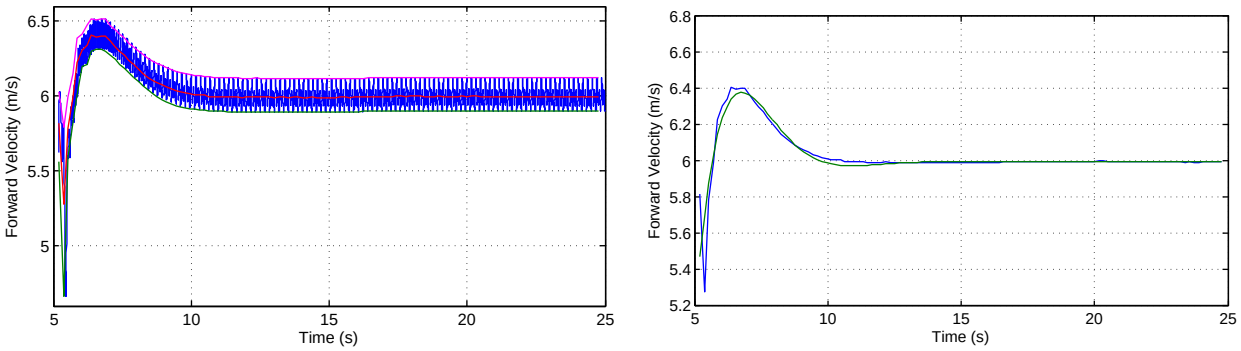

(a) Extraction of simple signals.

(b) Nonlinear least squares fit.

Figure 8. Dissociation of timescales.

which make it unlikely that such parameters will usable as true inputs for a simple input-output model of slow dynamics. At best, the specific values of the parameters will show up as part of a simple state-space model for slow dynamics, not just as an input. Given these preliminary results, analytical investigations for the purposes of describing omega limit sets and convergence properties may be the only way to close the book on potential input-output behavior of complicated system driven by oscillatory exosystems.

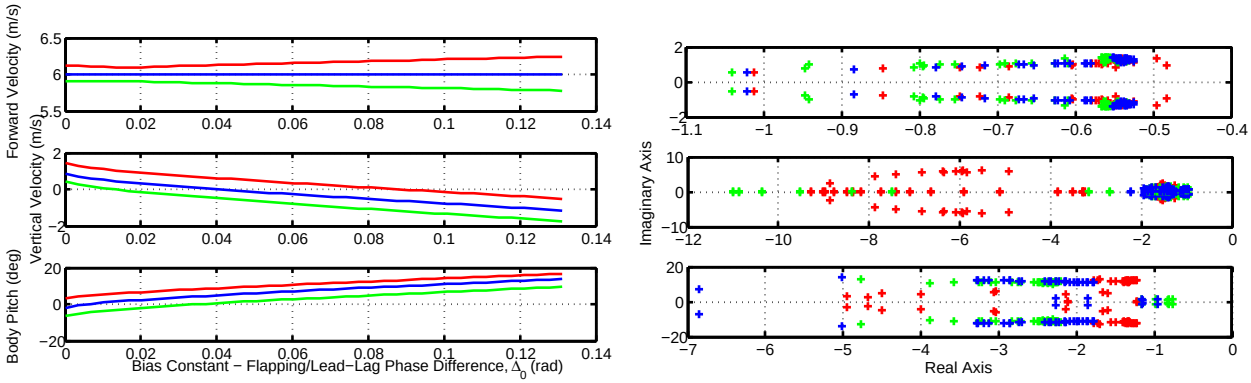

(a) Steady-State Behavior.

(b) Fitted Transient Eigenvalues.

Figure 9. Dissociation of Slow Dynamics.

V. Perspectives on Wingtip Motion

Studies of biological fliers investigate the wing kinematics in-depth.[12] They track up to 20 joint angles, which describe very complex motion.[26] This simulation does not yet have that level of complexity. However, we can begin looking at key indicators to ensure our model qualitatively resembles the wing motion of actual fliers. One of the key indictors presented in Tian, et al.[12] is wingtip motion. Their experiments were performed with a live bat in close to level flight. Therefore, we run a new simulation, do not initiate a turning maneuver, and take the wingtip data from the steady-state portion of the flight. In order to make a full comparison, we plot wingtip motion in the same mannar as Tian, et al.,[12] as well as the deviations from forward velocity in Fig. 10.

Most notably, the y-motion of the wingtip follows a path on the upstroke similar to the downstroke. This is because the model only has one rigid wing. Rather than progress down the path of strict mimicry, we take the first step of simply adding a single joint in the wing. The dynamic model follows a generalization given

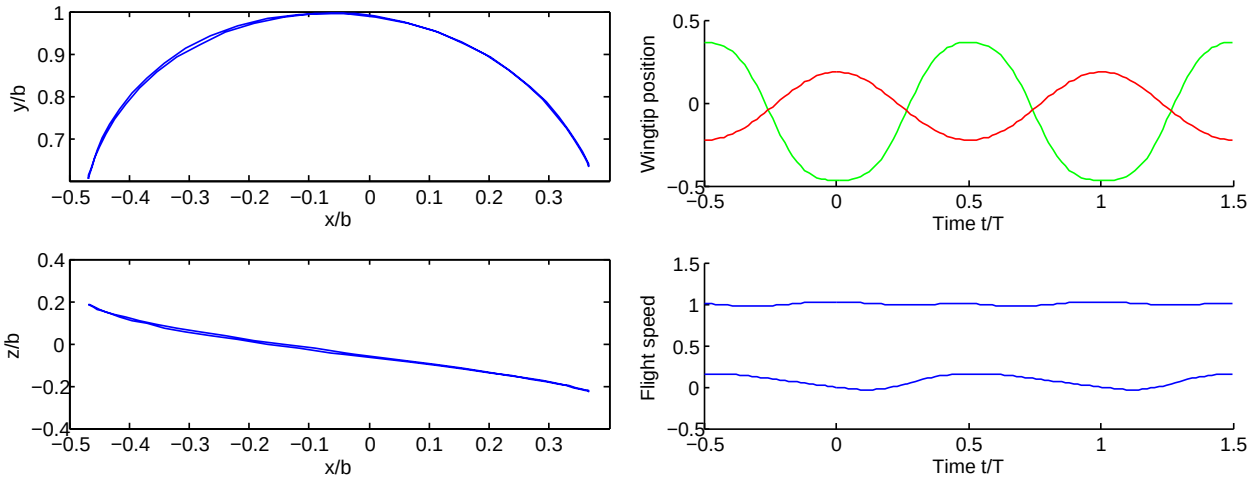

(a) Wingtip motion in planes.

(b) Wingtip position and flight speeds.

Figure 10. Simulated wingtip motion.

by Chung.[1] We calculate the local flow by

$$\begin{pmatrix} V_{wx} \\ V_{wy} \\ V_{wz} \end{pmatrix} = \mathbf{T}_{ws}(\phi_w, \psi_w)\mathbf{T}_{sb}(\Theta_s)(\mathbf{V}_b + \mathbf{\Omega}_b \times \mathbf{d}) + \tag{21}$$

$$(\mathbf{T}_{ws}(\phi_w, \psi_w)\mathbf{\Omega}_{tot}) \times \left(\begin{pmatrix} 0 \\ r_1 \\ 0 \end{pmatrix} + (r - r_1) \begin{pmatrix} 0 \\ -\cos\phi_2 \\ \sin\phi_2 \end{pmatrix} \right) + (r - r_1)\,\dot{\phi}_2 \begin{pmatrix} 0 \\ \sin\phi_2 \\ \cos\phi_2 \end{pmatrix}$$

where r_1 is the location of the joint and ϕ_2 is the angle between the two wing segments.

Further adjustments involve rotating the differential force added by blade elements beyond the joint and computing the correct moment arm. The force rotation is obvious and the moment arm is computed as

$$\mathbf{p}(r) = \mathbf{T}_{bs}(\Theta_s)\mathbf{T}_{sw}(\phi_w, \psi_w) \left[\begin{pmatrix} 0 \\ r_1 \\ 0 \end{pmatrix} + (r - r_1) \begin{pmatrix} 0 \\ -\cos\phi_2 \\ \sin\phi_2 \end{pmatrix} \right] \begin{pmatrix} d_x \\ d_y \\ d_z \end{pmatrix}. \tag{22}$$

Parameters of the second joint CPG were selected to approximate the motions observed by Iriarte-Diaz.[27] The simulation was unstable and no stable combination of parameters was found. Analytical investigations into the flight dynamics impacts of the second joint do not currently provide an explanation for this or a method for stabilizing such a flier. It remains open whether the best course of action is to investigate a jointed wing analytically or rely on numerical investigations of more detailed bat wing models. Without a stable simulation, we can not yet postulate on the wingtip motion of such a system with a jointed wing. This highlights the key need for an analytical test concerning the exosystem-based excitation of a multi-dimensional dynamic system.

VI. Conclusion

Stability and control of engineered flapping flight is a complicated, highly oscillatory problem. Central pattern generators are a convenient mathematical tool for generating oscillatory motion in a controlled, synchronous fashion. CPG arrays formed from coupled Hopf oscillators can be used to stabilize and control both longitudinal and lateral aircraft modes. However, the problem is far from answered. The key challenge going forward is to analytically describe how a complicated system will behave when excited by such an oscillatory exosystem. Most analytical methods fail for all but the simplest systems, as Poincaré-Bendixson will not apply to anything but a one-dimensional system excited by a one-dimensional exosystem. While numerical results show that stabilizing controllers can be found and that fast periodic motions might be

dissociable from slower motion, it is likely that this type of reasoning can not be applied broadly to the case of bat-scale flapping flight. Much additional work is needed to describe the global behavior of such problems.

A. Appendix: Simplified Longitudinal Equations

This appendix describes a simplified form of flapping flight equations, not for accurate mimicry, but for the purpose of making future analytical contributions more accessible.

A.A. Driving Exosystem and Equations of Motion

In order to derive the simplest form of a flapping flight system for analytical purposes, we will assume the CPG array has converged to a limit cycle and that there is no reflex arc which disturbs this convergence. As such, we assume the wing motions have converged to the perfect sinusoid

$$\phi = A\sin\omega t \quad \psi = B\sin\omega t + \Delta \quad \theta_w = C\cos\omega t \tag{23}$$

where ϕ is the symmetric flapping angle, ψ is the lead-lag angle, and θ_w is the wing pitch angle. The wing is assumed to be rigid, so these parameters are sufficient.

Following the typical method for equations of motion in Etkin[28] and Fan,[29] we can derive

$$\begin{aligned}
\dot{V} &= \frac{1}{m}\left[X\cos\alpha + Z\sin\alpha\right] - g\sin\gamma \\
\dot{\alpha} &= q - \frac{1}{mV}\left[X\sin\alpha - Z\cos\alpha\right] + \frac{g}{V}\cos\gamma \\
\dot{q} &= \frac{M}{I_y} \\
\dot{\theta} &= q.
\end{aligned} \tag{24}$$

In this form, we are assuming everything is symmetrical and have taken X and Z to be the force of lift and drag, in the body frame, on a single wing. These appear simple, but the expansions of X and Z are complicated, as is seen in our previous paper. In order to make the form as simple as possible while retaining key functionality for testing our hypothesis, we make the following assumptions:

1. The center of pressure on the wing is at a constant location through the flapping motion.

2. The lift and drag coefficients remain in the linear range for this particular c_p. Furthermore, the corresponding angle of attack can be computed for a single, fixed point. In general, there is no reason for these points to coincide. For the purpose of this study, we assume they do.

3. Induced velocity due to wing motion can be linearly superimposed. This is equivalent to a small-angle approximation and will be explained in the next section.

A.B. Local Velocity Calcualation

Following our previous paper and considering only the motions described above, we can derive the local flow velocity due to wing motions. We first assume that the body angular velocity is low, so that the only induced velocity effects are from flapping and lead-lag motions. Then, using

$$\mathbf{V}_w = \mathbf{T}_{wb}\mathbf{V}_b \tag{25}$$

we can obtain

$$\begin{aligned}
\mathbf{V}_{w,x} &= V\left[\cos\alpha\cos\psi + \sin\alpha\sin\psi\sin\phi\right] + r\dot{\psi} \\
\mathbf{V}_{w,z} &= V\sin\alpha\cos\phi - r\dot{\phi}\cos\psi.
\end{aligned} \tag{26}$$

Notice that a small angle assumption, $\phi \approx 0$ and $\psi \approx 0$, gives the expression one would expect if the wing motions were uncoupled, i.e. if each wing motion produced an induced velocity independently. We will make this assumption for further simplicity. Then, again using the same approach as before, we obtain

$$\beta_w = \arctan\frac{V\sin\alpha + r\dot{\phi}}{V\cos\alpha + r\dot{\psi}} \tag{27}$$

and

$$\alpha_w = \beta_w + \theta_w \tag{28}$$

with r denoting the length to the center of pressure for a straight wing. This formulation retains the fact that we can have induced velocity from each of the motions, which is necessary for thrust generation by proper turning of the resultant force vector.

A.C. Forces and Moments

Calculations of X and Z still follow the scheme of rotations from Section II.C. We obtain

$$\begin{aligned} X &= \cos\psi\left(-D\cos\beta_w - L\sin\beta_w\right) + \sin\psi\sin\phi\left(D\sin\beta_w - L\cos\beta_w\right) \\ Z &= \cos\phi\left(D\sin\beta_w - L\cos\beta_w\right). \end{aligned} \tag{29}$$

Now, we rely on assumption (2) from Section A.A and assume

$$\begin{aligned} L &= \frac{1}{2}\rho V_w^2 S C_L \alpha_w \\ D &= \frac{1}{2}\rho V_w^2 S C_D \alpha_w. \end{aligned} \tag{30}$$

The moment, M, is easily computed using the familiar relation

$$\mathbf{r} = \mathbf{T}_{bw}\begin{pmatrix} 0 \\ r \\ 0 \end{pmatrix} + \mathbf{d} = \begin{pmatrix} r\sin\psi\cos\phi \\ r\cos\phi\cos\psi \\ -r\sin\phi \end{pmatrix} + \mathbf{d} \tag{31}$$

with $\mathbf{d}$ representing the distance from the center of gravity to the wing root.

This system is the simplest form of an unsteady flapping flight system. It is a four-dimensional system driven by a three-dimensional exosystem. If one makes a feedback assumption, that is

$$\begin{pmatrix} A \\ B \\ C \\ \omega \\ \Delta \end{pmatrix} = f(V, \alpha, q, \theta), \tag{32}$$

then it is simply a very oscillatory four-dimensional system. Even in this simplified form, Poincaré-Bendixon does not apply, and an analytical solution is still open.

References

[1]Chung, S.-J. and Dorothy, M., "Neurobiologically Inspired Control of Engineered Flapping Flight," *AIAA Journal of Guidance, Control, and Dynamics*, Vol. 33, No. 2, 2010, pp. 440–453.

[2]Mueller, T. J., *Fixed and Flapping Wing Aerodynamics for Micro Air Vehicle Application*, Progress in Astronautics and Aeronautics, AIAA, 2001.

[3]Shyy, W., Lian, Y., Tang, J., Viieru, D., and Liu, H., *Aerodynamics of Low Reynolds Number Flyers*, Cambridge University Press, New York, NY, 2008.

[4]Azuma, A., *The Biokinetics of Flying and Swimming*, AIAA, 2nd ed., 2006.

[5]Kato, N. and Kamimura, S., *Bio-Mechanisms of Swimming and Flying: Fluid Dynamics, Biomimetic Robots, and Sports Science*, Springer Verlag, 2008.

[6]Norberg, U. M., *Vertebrate Flght: Mechanics, Physiology, Morphology, Ecology and Evolution*, Springer-Verlag, 1989.

[7]Dickinson, M. H., Lehmann, F. O., and Sane, S. P., "Wing Rotation and the Aerodynamic Basis of Insect Flight," *Science*, Vol. 284, 1999, pp. 1954–1960, June.

[8]Dickinson, W. B. and Dickinson, M. H., "The Effect of Advance Ratio on the Aerodynamics of Revolving Wings," *Journal of Experimental Biology*, Vol. 207, 2004, pp. 4269–4281.

[9]Tatjana Y. Hubel, Nickolay I. Hristov, S. M. S. K. S. B., "Time-resolved wake structure and kinematics of bat flight," *Exp Fluids*, Vol. 46, 2009, pp. 933–943.

[10]Wang, Z. J., "Vortex Shedding and Frequency Selection in Flapping Flight," *Journal of Fluid Mechanics*, 2000, pp. 323–341, 410.

[11]Oppenheimer, M. W., Doman, D. B., and Sigthorsson, D. O., "Dynamics and Control of Minimally Actuated Biomimetic Vehicle: Part II - Control," *AIAA Guidance, Navigation, and Control Conference*, Chicago, IL, Aug. 2009, AIAA Paper 2009-6161.

[12]Tian, X., Iriarte-Diaz, J., Middleton, K., Galvao, R., Israeli, E., Roemer, A., Sullivan, A., Song, A., Swartz, S., and Breuer, K., "Direct Measurements of the Kinematics and Dynamics of Bat Flight," *Bioinspiration and Biomimetics*, Vol. 1, 2006, S10-S19.

[13]Seo, K., Chung, S.-J., and Slotine, J.-J. E., "CPG-based Control of a Turtle-like Underwater Vehicle," *Autonomous Robots*, 2010, Control of Locomotion: From Animals to Robots.

[14]Isidori, A. and Byrnes, C., "Steady-state behaviors in nonlinear systems with an application to robust disturbance rejection," *Annual Reviews in Control*, Vol. 32, 2008, pp. 1–16.

[15]Strogatz, S., *Nonlinear Dynamics and Chaos With Applications to Physics , Biology, Chemistry, and Engineering*, Perseus Books Group, Cambridge, MA, 1994.

[16]Bernd Krauskopf, Hinke M. Osinga, J. G.-V. E., *Numerical Continuation Methods for Dynamical Systems*, Springer, 2007.

[17]Slotine, J.-J. E. and Li, W., *Applied Nonlinear Control*, Prentice Hall, 1991.

[18]Chung, S.-J. and Slotine, J.-J. E., "Cooperative Robot Control and Concurrent Synchronization of Lagrangian Systems," *IEEE Transactions on Robotics*, Vol. 25, No. 3, 2009, pp. 686–700.

[19]Roberts, A., Soffe, S., Wolf, E., Yoshida, M., and Zhao, F., "Central Circuits controlling locomotion in young frog tadpoles," *Ann. N.Y. Acad. Sci.*, Vol. 860, 1998, pp. 19–34.

[20]Tytell, E. D. and Cohen, A. H., "Rostral Versus Caudal Differences in Mechanical Entrainment of the Lamprey Central Pattern Generator for Locomotion," *J. Neurophysiol.*, Vol. 99, 2008, pp. 2408–2419.

[21]Grillner, S., "Neurological Bases of Rhythmic Motor Acts in Vetebrates," *Science*, Vol. 228, 1985, pp. 143–149.

[22]Kiehn, O., "Locomotor Circuits in the Mammalian Spinal Cord," *Annual Review of Neuroscience*, Vol. 29, 2006, pp. 279–306.

[23]Brocard, F., Tazerart, S., and Vinay, L., "Do Pacemakers Drive the Central Pattern Generator for Locomotion in Mammals?" *The Neuroscientist*, Vol. 16, 2010, pp. 139–155.

[24]Ellington, C., "The Aerodynamics of Hovering Insect Flight. I-VI," *Philosophical Transactions of the Royal Society of London B Biological Sciences*, Vol. 305, 1984, pp. 1–181.

[25]Hedrick, T. L. and Biewener, A. A., "Experimental Study of Low Speed Turning Flight in Cockatoos and Cockatiels," *45th AIAA Aerospace Sciences Meeting and Exhibit*, Reno, NV, January 2007.

[26]Riskin, D. K., Willis, D. J., Iriarte-Diaz, J., Hendrick, T. L., Kostandov, M., Chen, J., Laidlaw, D. H., Breuer, K. S., and Swartz, S. M., "Quantifying the Complexity of Bat Wing Kinematics," *Journal of Theoretical Biology*, Vol. 254, 2008, pp. 604–615.

[27]Iriarte-Diaz, J. and Swartz, S. M., "Kinematics of slow turn maneuvering in the fruit bat Cynopterus brachyotis," *Journal of Experimental Biology*, Vol. 211, 2008, pp. 3478–3489.

[28]Etkin, B. and Reid, L. D., *Dynamics of Flight*, 3rd ed., 1996, John Wiley and Sons, Inc.

[29]Fan, Y., Lutze, F. H., and Cliff, E. M., "Time-Optimal Lateral Maneuvers of an Aircraft," *AIAA Journal of Guidance, Control, and Dynamics*, Vol. 18, 1995, pp. 1106–1112.